Elastic Wind-Tunnel Models for Predicting Longitudinal Stability Derivatives of Elastic Airplanes

J. ROSKAM*
University of Kansas, Lawrence, Kansas

AND

T. HOLGATE† AND G. SHIMIZU‡
The Boeing Company, Seattle, Wash.

The objective of this investigation was the development of elastic wind-tunnel models to be used in predicting stability derivatives for elastic airplanes, in particular the SST. A novel feature of these models is that they were tested at full-scale dynamic pressures. Scaling laws, manufacturing problems, and testing problems encountered during this development are brought out. The differences between jig shape and design shape of an elastic airplane are illustrated, using the Boeing SST as an example. Application and use of elastic model data to the prediction of full-scale airplane lift and pitching-moment characteristics are presented. Correlation data between theoretical predictions for longitudinal stability and control derivatives and experimental measurements on elastic models are given. These results clearly demonstrate the practicality of elastic models for tests at full-scale dynamic pressures.

Nomenclature

C_p = pressure coefficient, P/qS_w
P = aerodynamic load, $P_L - P_u$, lb
q = dynamic pressure, psf
S_w = reference (wing) area, ft²
E = Young's modulus, psf
I = bending moment of inertia, ft⁴
G = shear modulus, psf
J = torsion moment of inertia, ft⁴
C = chord, ft
C_L = lift coefficient L/qS_w
C_M = moment coefficient M/qSc_R
α = angle of attack, deg
δ = scaled or actual deflection, ft
F = structural influence coefficient, δ/unit load
y = span station, l
ac = airplane aerodynamic center X (ref. point)$/C_R - (dC_M/dc_L) \times 100 \approx \%C_R$
$C_{L\alpha}$ = airplane lift-curve slope
n = airplane load factor = $C_{LA}qS_w/W$
Λ = sweep angle of wing leading edge
b = wing span, ft
Δac = aerodynamic center increment, $ac_E - ac_R$

Subscripts

R = root chord, or rigid
E = elastic
0 = zero angle of attack applied to lift, or zero lift applied to moments
$m=0$ = zero-mass term
$\partial|_q$ = derivative at constant dynamic pressure
$\partial|_n$ = derivative at constant load factor or g
CTW = force or moment due to camber and twist

1. Introduction

THE purpose of this article is to discuss the development and application of a recently developed technique in constructing elastic wind-tunnel models. These elastic models are tested at full-scale dynamic pressures. They are used in the prediction of steady-state aeroelastic effects on stability, control, and performance for the Boeing SST.

Section 2 presents general discussion of the purpose of elastic model testing. Scaling laws needed for the design of elastic models suitable for testing at full-scale dynamic pressures are discussed in Sec. 3.

A description of a typical elastic model used in the Boeing SST development program is the subject of Sec. 4. Construction techniques used for this model are illustrated. The differences between jig (wind-off) shape and design (wind-on, cruise flight condition) shape are shown to be significant. In Sec. 5, a discussion is given of some typical aerodynamic results from elastic model tests.

The application and use of elastic model data to the prediction of full-scale airplane lift and pitching-moment characteristics are presented in Sec. 6. Graphical procedures used in predicting full-scale $C_L - \alpha$ and $C_L - C_m$ curves from elastic model data are discussed.

In designing elastic models and using elastic model data, it is necessary to employ rather complicated computer programs based on matrix solutions of the steady-state equations of motion of the elastic airplane. This is done by using structural and aerodynamic influence coefficient methods. To indicate the accuracy of these theoretical methods, a correlation between predicted model behavior and measured model behavior in lift and pitch is presented in Sec. 7. Conclusions are given in Sec. 8.

2. Objectives for Elastic Model Testing at Full-Scale Dynamic Pressures

Objectives in testing elastic models at full-scale dynamic pressures are to study and determine 1) elastic airplane shape changes, 2) changes in performance, stability, and control parameters induced by elastic shape changes, and 3) verification of theoretical predictions of aeroelastic effects on performance, stability, and control parameters.

In modern airplane design, structural aspects are not governed by strength alone; they are also governed by stiffness. The factor of stiffness of the airplane structure becomes a dominant factor with very large airplanes flying at high dynamic pressures. Reduction in stiffness not only changes the dynamic characteristics of the airplane, such as flutter and vibration, but it also changes several important

Presented as Paper 68-56 at the AIAA 6th Aerospace Sciences Meeting, New York, January 22–24, 1968; submitted February 8, 1968; revision received June 24, 1968.

* Formerly Senior Group Engineer, Supersonic Transport Branch, The Boeing Company; now Associate Professor, Aerospace Engineering. Associate Fellow AIAA.

† Research Specialist, Supersonic Transport Branch. Member AIAA.

‡ Aerodynamics Engineer, Supersonic Transport Branch.

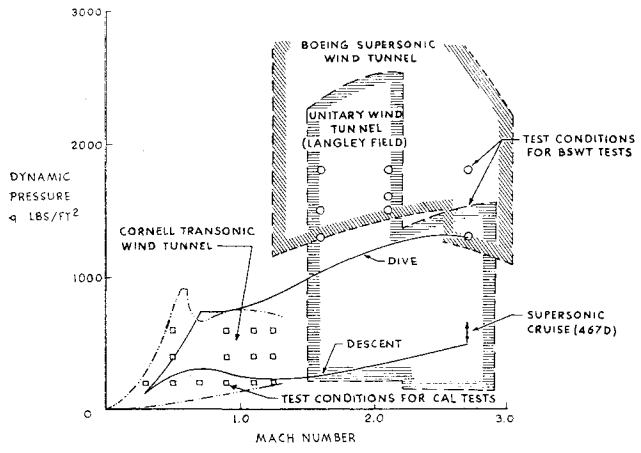

Fig. 1 Dynamic pressure comparison; Langley, Cornell, and Boeing.

static aerodynamic characteristics, such as performance, stability, and control. It is important to determine the effects of static aeroelasticity experimentally through the use of elastic models.

Flutter models cannot be used for the type of testing implied here. For one thing, these models are scaled for both mass and stiffness, which makes them rather flimsy and precludes testing at full-scale dynamic pressures and Mach numbers. The problem, therefore, was to build an elastic model with properly scaled stiffness characteristics, yet strong enough to withstand full-scale dynamic pressures and Mach numbers.

The reasons for objectives 1–3 will now be discussed in more detail. The first objective is to measure and observe in the wind tunnel actual airplane shape changes as a result of changing dynamic pressures and Mach numbers. In the case of airplanes that experience large shape changes, it is important to know accurately the shape in which the airplane has to be built in its assembly jigs so that it can deflect into its proper optimum shape at some design cruise weight, dynamic pressure, and Mach number. Because the design and construction of elastic models create problems quite similar to those encountered on the real airplane, these models can serve to identify the accuracy with which jig shapes can be determined from a specified cruise shape.

The second objective for testing a flexible model is to study and determine aeroelastic effects on performance, stability, and control characteristics of the airplane. However, because of its constant 1-g environment, the flexible model will not simulate the airplane exactly; Sec. 6 of this article deals with this problem. The flexible model can be used to measure the effectiveness of various control surfaces that are vitally affected by the complicated intercoupling of structural and aerodynamic phenomena. Control surfaces that have been tested on flexible models are elevators, elevons, spoilers, and ailerons. The flexible model can also simulate hard-to-calculate situations, for example, the effect of shear ties between wing and tail, such as exist on the Boeing SST. Finally, visual effects by use of oil-flow tests, wing-deflection photos, and high-speed movies help in predicting and interpreting aeroelastic characteristics of the airplane.

The third objective in determining the airplane flexibility characteristics by model experiment is to substantiate theoretical predictions and analyses. It is obviously necessary to obtain an appreciation of how well predictions based on computer programs compare with test data. This is true not only for the absolute force and moment characteristics, but also for elastic increment comparisons. Once the computer analysis has been checked and a proper correlation has been made, it is possible to predict elastic effects for many flight conditions quickly and inexpensively. Having stated the reasons and objectives for elastic model testing at full-scale Mach number and dynamic pressure, the techniques used in model-scaling design and construction are now discussed in Secs. 3 and 4.

3. Model-Scaling Laws

The way in which a tunnel model is scaled depends largely on the test objectives. Generally, it is the objective of the experimenter to establish aerodynamic similarity in some flight regime between the model he is testing and the airplane it represents. In the case of rigid airplanes this is done by building a rigid, geometrically scaled model and testing it at full-scale Mach numbers. The test dynamic pressures are important insofar as they establish the Reynolds number.

To simulate on model scale the lift, drag, and moment characteristics of elastic airplanes, it suffices to simulate static load-deflection relationships on the model. It is not necessary to simulate structural dynamic response of the airplane. The following definition is basic to the development of the scaling laws used for this type of flexible model:

Definition: The flexibility of model and airplane is similar when a nondimensional lift distribution $C_p(x,y)$ produces the same nondimensional deflection $\delta/(S_w)^{1/2}$, where δ = scaled or actual deflection and S_w = scaled or actual wing area. The aerodynamic load on any elementary area S_i located at a given panel point (i) is

$$P_i = qC_{P_i}(\Delta S_i/S_w)S_w \tag{1}$$

This load produces a deflection δ_{ji} at any other arbitrary point j. If the structure deflects linearly, it is possible to write the deflection at the point (j) as

$$\delta_{ji} = F_{ji}P_i \tag{2}$$

where F_{ji} is the deflection at j due to a unit load at i, also called a structural influence coefficient. The nondimensional deflection at j would then be

$$\delta_{ji}/(S_w)^{1/2} = F_{ji}qC_{P_i}(\Delta S_i/S_w)[S_w/(S_w)^{1/2}] \tag{3}$$

Neglecting the effect of Reynolds number on C_{P_i}, there will be aerodynamic flow similarity (equal C_{P_i}) between airplane and model if the model is tested at the same Mach number. Furthermore, there is implied geometric similarity between the airplane and the model, which means equal $\Delta S_i/S_w$. For these reasons, the flexibility of the model will be similar to that of the airplane when the following is satisfied:

$$(q_M/q_A)(F_M/F_A)(Sw_M/S_{w_A})^{1/2} = 1 \tag{4}$$

where M = model and A = airplane. The subscripts j and i have been dropped. Assuming that the wing acts as a cantilevered beam, the influence coefficient F results from bending and torsion of the elastic axis. First, consider bending. It can be shown from beam theory that the influence coefficient F is proportional to S_w and EI such that

$$F \cong S_w^{3/2}/EI \tag{5}$$

Substituting into Eq. (4) the condition for similarity of beam bending yields

$$(q_M/q_A)(E_A/E_M)(I_A/I_M)(S_{w_M}/S_{w_A})^2 = 1 \tag{6}$$

Second, consider torsion. Similar reasoning will show that the following relation must be satisfied for similarity of beam torsion:

$$(q_M/q_A)(G_A/G_M)(J_A/J_M)(S_{w_M}/S_{w_A})^2 = 1 \tag{7}$$

Combining Eqs. (6) and (7), it follows that the condition of similarity for a flexible model is

$$(J/I)_M(G/E)_M = (J/I)_A(G/E)_A \tag{8}$$

The ratio G/E is almost independent of the materials normally chosen for model construction. Therefore, Eq. (8)

reduces to

$$(J/I)_M = (J/I)_A \tag{9}$$

almost regardless of the material from which the model is built.

Returning to Eq. (6), the model-airplane geometric scale factor $(S_{w_M}/S_{w_A})^{1/2}$ is usually determined by the size of the wind-tunnel test section. The scale factor q_M/q_A is determined by comparing flight-dynamic pressure with those obtainable in test facilities. Figure 1 presents a typical comparison. It appears that the model can be scaled such that $(q_M/q_A) = 1$, which means equal dynamic pressure for airplane and model. Once the model scale and the dynamic pressure scale have been selected, the J/I scale is fixed. The next problem then is to keep the resulting wing-beam geometry within the airfoil contour of the model wings and tail. Considerable latitude is available in meeting this boundary condition if high-strength steel is used. This is because a solid section generally has far too much bending and torsion stiffness. A typical model wing is then machined out of solid steel. Machining of cutouts and notches in the solid wing results in a multifingered spar, as will be shown in the next section. By adjusting the depth of cutouts and notches, it is possible to obtain the desired values of EI and GJ and their corresponding JG/EI ratios. A filler material is inserted between the wing-beam fingers. This induces some bending and torsional stiffness changes, and this fact has to be accounted for in the design of the model wing.

4. Wind-Tunnel Model

4.1 Model Description

One model that has been used to measure the effect of aeroelasticity on lift, drag, and pitching moment is shown in Fig. 2. This model was designed with a rigid fuselage and elastic wing and horizontal tail. A rigid model was available for comparison. The elastic wing and tail panels were interchangeable with corresponding rigid wing and tail panels so that either a rigid or elastic configuration could be tested. The shape of the rigid model configuration was selected to conform to the 1-g cruise (design) shape of the airplane. A 1-g cruise shape is defined as that shape of the airplane which is recommended at a specific Mach number, dynamic pressure, and fuel-payload flight condition (design-point condition). This shape is tailored to achieve a high L/D ratio and was dictated largely by performance and static stability considerations.

The elastic model configuration with the elastic outer wing and tail panels has an exterior shape that depends on the aerodynamic loading. Both elastic wing and tail were scaled in bending and torsional stiffnesses in accordance with the

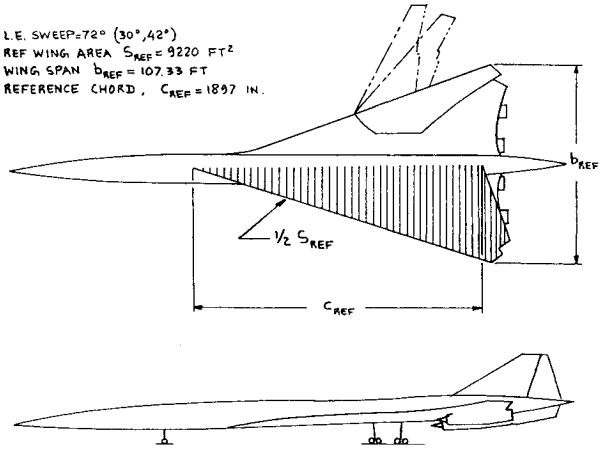

Fig. 2 Typical SST general arrangement.

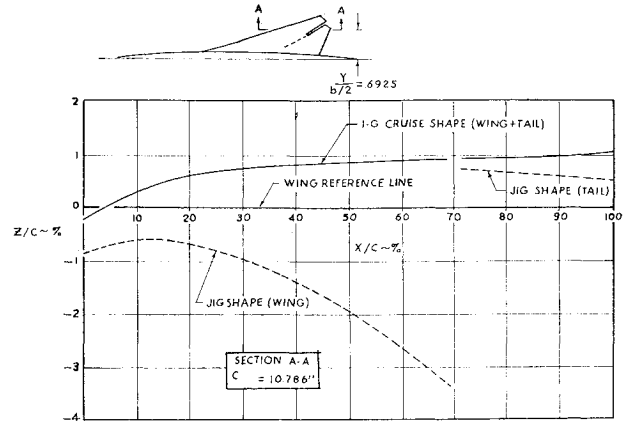

Fig. 3 Comparison between model 1-g cruise shape and jig shape.

scaling rules of Sec. 3. The 1-g (design) cruise shape of the elastic model configuration can be achieved in the wind tunnel only when subjected to the design-point Mach number, dynamic pressure, and angle-of-attack condition. At any other Mach number and dynamic-pressure conditions, the elastic configuration has a shape that is deflected away from the cruise shape. The elastic model is manufactured to the so-called jig shape.

The jig shape is defined as that shape of the airplane when all aerodynamic, thrust, and inertial loads of the design-point condition are removed; it is the shape to which an airplane is constructed in a final assembly jig. Figure 3 shows a typical comparison between the 1-g cruise shape (design-point camber) and corresponding jig shape (jig camber) at one span station. It may be seen that the differences between the two shapes are significant. Observe that an elastic wind-tunnel model has a jig shape different from that of the airplane, largely because neither airplane mass nor mass distribution are simulated by the model.

4.2 Model Construction

Manufacture of the elastic wing began by cutting the general contour of the jig wing panel from a cast steel block. Next, the upper and lower surfaces were cut separately by a Rockford machine guided along a Rockford pattern, so that the final product conformed to a precalculated jig camber and twist distribution. After both upper and lower surfaces of the elastic panel were smoothed, the wing spar section was worked on. This involved cutting and removing a correct amount of steel from both upper and lower surfaces along a defined spar location (elastic axis), so that it would have the predetermined spar cross-sectional area and shape for various spar stations, as shown in Fig. 4a. Next, slots are cut at a regular interval perpendicular to the spar, starting from both leading and trailing edges. The slot depth is such that the desired spar width is maintained, as shown in Fig. 4b. Finally, the slots are filled with plastic filler material that does not bulge and has the right kind of adhesive qualities for the test environment.

The spar of the elastic wing represents the elastic axis and the major part of the bending and torsional stiffness. The local stiffness is controlled by the shape and size of the local spar section. Allowance must be made on spar design to account for the small increase in stiffness due to the plastic filler material, so that the final elastic jig panel will have the required stiffness distribution. This involves some iteration between calibrating and manufacturing.

Figure 5a shows the top view of the assembled elastic model configuration. The wing and tail spars have been painted black. Figure 5b shows the front-side view of the assembled elastic configuration; observe the gap between wing and tail in this model jig shape. Figure 5c shows a side

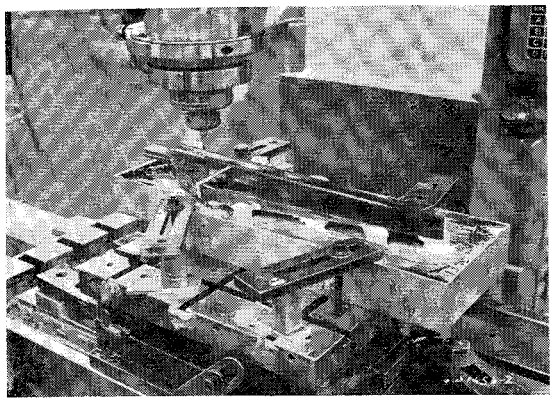

a) Upper surface

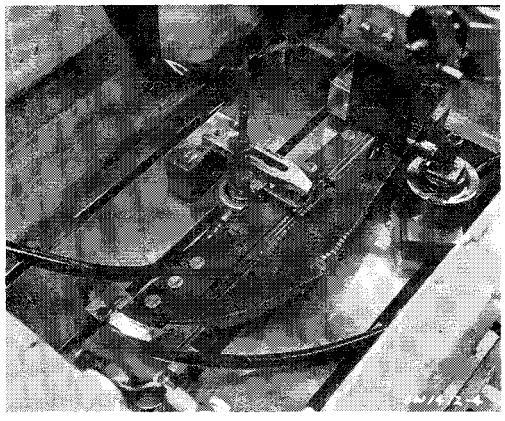

b) Slots

Fig. 4 Machining of elastic wing.

view of the assembled elastic configuration forced to represent the 1-g cruise shape. This is the shape assumed by the model when placed in the wind tunnel at the design cruise flight condition, i.e., the proper Mach number, dynamic pressure, and angle of attack.

5. Testing Conditions and Typical Aerodynamic Results

Figure 1 shows an overlay of the envelope of SST flight-dynamic pressures vs Mach number with the dynamic pressures of several wind-tunnel facilities that can be used to conduct elastic model testing. The SST flight envelope has a Mach number range between 0 and 2.7 and a dynamic-pressure range between 0 and approximately 1250 psf. To examine and acquire data on static aeroelastic effects for the entire SST flight envelope, it is necessary to test the elastic model in at least two pressure wind tunnels, such as Cornell's transonic and Langley's unitary wind tunnels. Testing at the Boeing supersonic wind tunnel is done to obtain aeroelastic information at very high dynamic pressures.

Typical examples of longitudinal aerodynamic characteristics obtained from tests in the Boeing supersonic wind tunnel and Cornell's transonic wind tunnel are presented in Figs. 6 and 7, respectively. These tests were conducted at Mach numbers from 0.3 to 2.7 and dynamic pressures of 200 to 1800 psf. The Reynolds number varied between 10^6 and 10×10^6 l/ft. Transition strips consisting of 30 to 40 grains/in. wide and located $\frac{1}{4}$ in. behind the leading edge were used on both surfaces of the wing.

Wind-tunnel data on an elastic model at a constant Mach number must be obtained for a range of dynamic pressures to be meaningful. Reynolds number varies in the process, but this is generally not serious. The effects of mass and mass distribution must be accounted for theoretically. As will be shown in Sec. 6, these effects turned out to be negligible on model scale.

From the data shown in Figs. 6 and 7, it is possible to obtain static aeroelastic incremental effects that are expressed either as a ratio or as an increment between elastic and rigid aerodynamic data. Typical of such data are the $C_{L\alpha_E}/C_{L\alpha_R}$ and Δac plots as shown in Figs. 8 and 9. These values can then be applied to correct the rigid wind-tunnel data. Procedures for doing this are discussed in Sec. 6. Photographs of the model taken during wind-tunnel tests are illustrated in Fig. 10.

6. Use of Elastic Wind-Tunnel Model Data in Predicting Full-Scale Elastic Airplane Characteristics

An important part of the work by the stability and control engineer is the use of wind-tunnel data in predicting full-scale airplane characteristics. Because of unknowns arising from Reynolds number effects, shock formations, and power effects, this problem has always been a difficult one, even in the case of rigid airplanes and models. If, in addition, the elastic effects of airplane and model must be accounted for, then the problems in using tunnel data to predict full-scale airplane characteristics multiply. The purpose of this section is to discuss step-by-step the procedure that should be followed in using elastic model data to predict full-scale airplane characteristics. In doing this, the fundamental differences that exist between an airplane in free flight and a model fixed in the tunnel are accounted for. These differences are listed in Table 1. The prediction of full-scale elastic lift-curve slope is discussed in Sec. 6.1. This is followed in Sec. 6.2 by a dis-

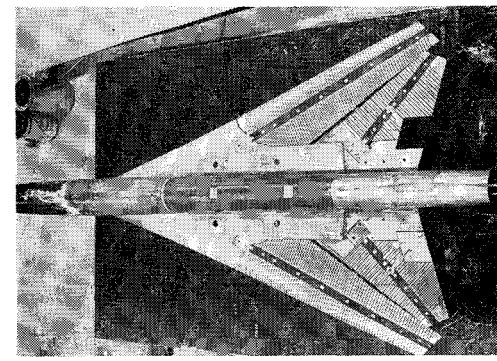

a) Top view

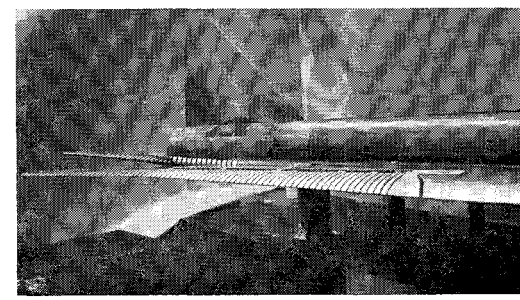

b) Front-side view (observe jig shape)

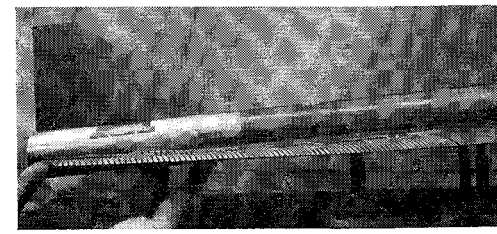

c) Side view (model forced into 1-g cruise shape)

Fig. 5 Assembled elastic model.

Table 1 Differences between an airplane and a wind-tunnel model

Airplane	Model
1) Load factor (n) varies with angle of attack	1) Model is tested at constant load factor ($n = 1$) when angle of attack is varied
2) Airplane is completely flexible Example: Wing, Tail, Body } Flexible	2) Model usually has only partial flexibility. Example: Body, Inboard wing and tail panels } Rigid Outboard wing and tail panels } Flexible
3) Weight distribution varies for various flight conditions	3) Weight distribution constant and not similar to any airplane distribution
4) Airplane experiences various changes in flexibility because of environmental changes (aerodynamic heating)	4) Model experiences changes in flexibility created by wind-tunnel temperatures

cussion of the prediction of full-scale elastic pitching moment vs lift coefficient. The procedures discussed in this section apply to cases where lift and pitching moment vary with angle of attack in a nonlinear manner.

6.1 Prediction of Lift Coefficient vs Angle of Attack from Elastic Model Data

This section describes four steps needed to predict the full-scale airplane $C_{L_A} - \alpha$ curve for a design flight condition. It is assumed that the shape of the airplane for the design flight condition is known (cruise shape) and that a rigid model has been constructed which is a scaled duplication of this shape. It is realized that rigid models cannot be perfectly rigid, and the consequence of this is discussed also.

The idea of building rigid models of the cruise shape relies on the assumption that one particular flight condition is of major importance or that the demonstration of analytical accuracy at one flight condition is sufficient to validate estimates for other conditions. It is impractical to construct rigid models for each important flight condition. When using the word airplane, the true (elastic) airplane is meant. When using the word rigid airplane, the airplane shape that results from freezing the airplane (true, elastic) in some equilibrium flight condition is meant.

Making the assumptions that the wind-tunnel model is a perfectly scaled duplication of the airplane, that Reynolds number effects and power effects are negligible, and that shock formations are properly simulated, the rigid airplane $C_{L_A} - \alpha$ curve should be identical to the measured rigid model $C_{L_M} -$

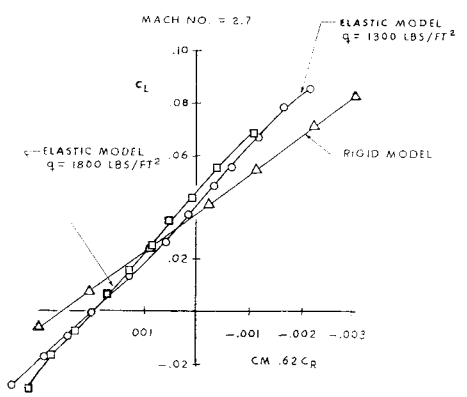

Fig. 6 Effect of dynamic pressure on pitching-moment curve.

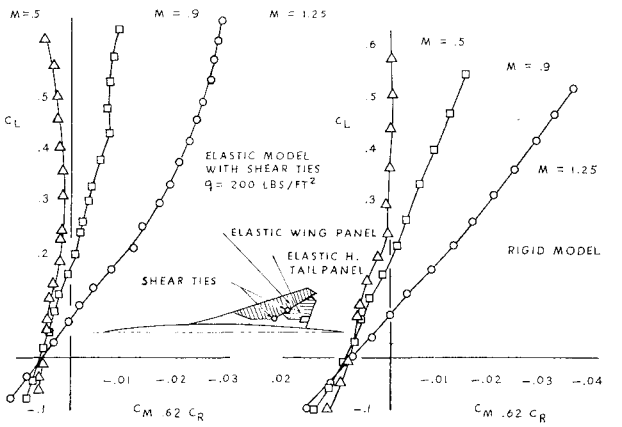

Fig. 7 Effect of Mach number on pitching-moment curve for rigid and elastic models.

α curve. This is indicated in Fig. 11 by the curves marked "rigid".

It is also assumed that an elastic model has been constructed which, when tested at cruise Mach number, cruise dynamic pressure, and cruise angle of attack, deflects to the desired cruise shape. This implies that the rigid and the elastic models have, for the design flight condition, identical values of C_L, C_m, and C_D at the design α. Figure 11 reflects this fact at point P_1. The result of wind-tunnel measurements then is the establishment of $C_{L_M} - \alpha$ curves for the rigid and elastic model. This completes step 1.

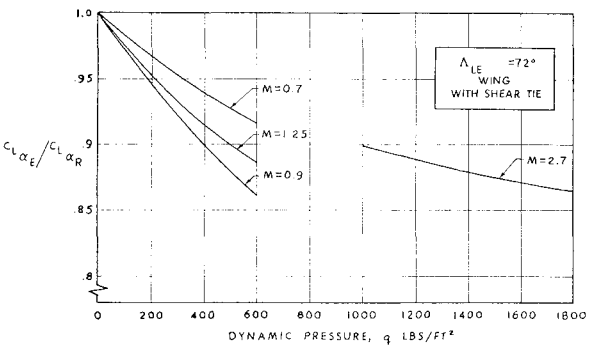

Fig. 8 Ratio of elastic to rigid lift-curve slope.

Observe that, while on the airplane, a variation of α at constant dynamic pressure implies a varying load factor; this is not so for the wind-tunnel model, where the load factor is always one. Even though this fact is of no consequence to rigid airplanes and models, for the elastic airplane it has the important consequence that inertial forces participate in deforming the airplane. The different effects of gravity on airplane and model can be accounted for by introducing the concept of zero airplane and model mass. Because $n = 1$ in

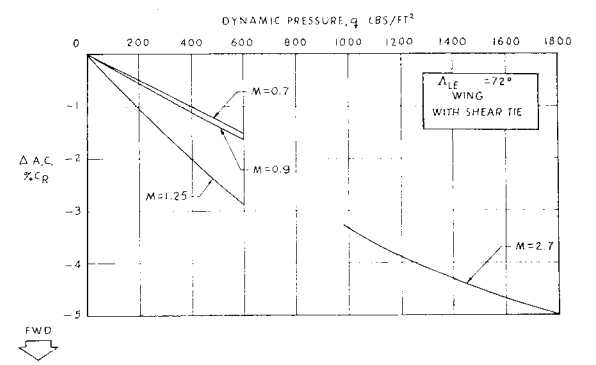

Fig. 9 Aerodynamic center movement between rigid and elastic model.

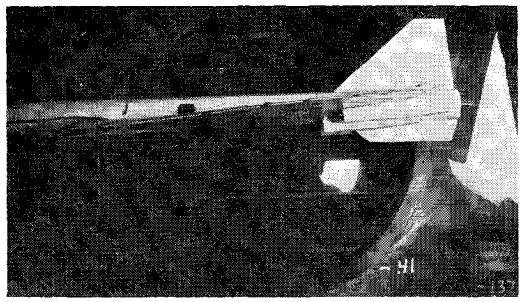

a) Mach 2.70, q = 1800 psf, α = +0.4°

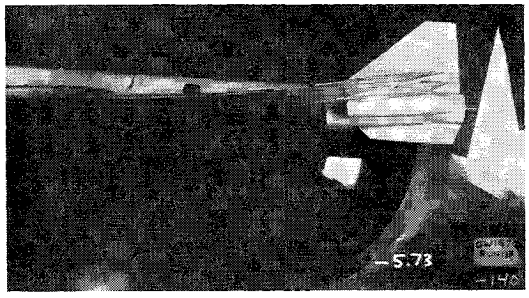

b) Mach 2.70, q = 1800 psf, α = +5.7°

Fig. 10 Relative shape of wing and tail.

the tunnel, correcting to zero model mass has the effect of shifting the elastic model $C_{L_M} - \alpha$ curve (vertically) over a small amount $\Delta C_{L_{M\ m=0}}$. This amount can be computed (from the known model mass and stiffness distribution), but is expected to be very small. A typical value computed for the current elastic SST model is $\Delta C_{L_{M\ m=0}} = 0.00031$ at $M = 2.7$ and $q = 456$ psf. This value is indeed small, compared with the flight C_L at this Mach number and dynamic pressure, which is $C_{L_{\text{design}}} = 0.085$.

It has been assumed that the effect of model mass on model elasticity (deflection) is constant over the α range. This assumption is reasonable, particularly in view of the smallness of $\Delta C_{L_{M\ m=0}}$. The zero-mass model $C_{L_M} - \alpha$ curve is now replotted on the left (i.e., airplane side of Fig. 11). This completes step 2.

For the airplane at the design angle of attack α_{design}, it is possible to compute $\partial C_{L_A}/\partial n$, the incremental lift coefficient due to airplane mass distribution at $n = 1$. This yields point P_2. Assuming that the elastic model is perfectly scaled (dimensional and stiffness) and that local shocks and Reynolds effects are negligible, it follows that the zero-mass airplane $C_{L_A} - \alpha$ curve should be identical to the zero-mass elastic model $C_{L_M} - \alpha$ curve, but shifted vertically so that it intercepts point P_2. This provides the first anchor point for prediction of full-scale characteristics and represents step 3.

Because the airplane in reality has mass and because load factor varies with α, it is necessary to correct the full-scale zero-mass $C_{L_A} - \alpha$ curve. Load factor is defined as

$$n = C_{L_A} qS_w/W \tag{10}$$

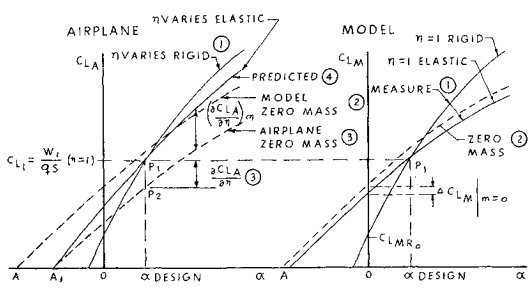

Fig. 11 Prediction of airplane lift-curve from elastic model data.

where W = weight. Notice that $n = 0$ for $C_{L_A} = 0$. Because of this, it is possible to consider the line $C_{L_A} = 0$ as corresponding to a zero-gravity environment. For that reason, the airplane $C_{L_A} - \alpha$ curves for full- and zero-mass intersect at $C_{L_A} = 0$ (point A_1), providing still another anchor point in the process of predicting full-scale airplane characteristics. The effect of load factor on the $C_{L_A} - \alpha$ curve is expressed by the increment

$$\Delta C_{L_{A_n}} = (\partial C_{L_A}/\partial n)n \tag{11}$$

Observe that $\partial C_{L_A}/\partial n$ for the airplane is a function of its known mass and stiffness distribution, dynamic pressure, and Mach number. It is assumed that the partial derivative $\partial C_{L_A}/\partial n$ has a value independent of α. In other words, it is assumed that the incremental aerodynamic loading due to mass distribution $\Delta C_{L_{A_n}}$ is not a function of the variation of lift distribution with an angle of attack. A typical value for $\partial C_{L_A}/\partial n$ is 0.0050, which, although small compared with the design C_{L_A} at $n = 1$, is not negligible. Adding the correction $\Delta C_{L_{A_n}}$, the full-scale $C_{L_A} - \alpha$ curve of the (elastic) airplane has finally been found. Notice that both points A_1 and P_1 are on the elastic airplane $C_{L_A} - \alpha$ curve. The correction ΔC_{L_A} varies from zero at A_1 to $\partial C_{L_A}/\partial_n$ at P_2, but in a linear manner. This completes step 4.

Note that:

1) It will be observed that the process of predicting full-scale airplane $C_{L_A} - \alpha$ characteristics from elastic model data involves computer applications, because it is not feasible to simulate mass and mass-distribution while at the same time testing at full-scale Mach number and dynamic pressures.

2) The procedures indicated here depend on a number of assumptions, the essentials of which are a) power, shock, and Reynolds number effects negligible (or accounted for separately), and b) $\Delta C_{L_{M\ m=0}}$, $\partial C_{L_A}/\partial n$ are independent of α.

3) The procedures indicated here can be applied at only one flight condition if, as is usually the case, only one rigid and one elastic model are available. For any other flight condition, the rigid model actually has the wrong shape. The correction procedure to be followed in that case is outlined below.

4) Notice that the (elastic) airplane lift-curve slope is made up of two components, as indicated by the following equation:

$$C_{L_{\alpha_A}} = \left.\frac{\partial C_{L_A}}{\partial \alpha}\right|_q = \left.\frac{\partial C_{L_A}}{\partial \alpha}\right|_n + \left.\frac{\partial C_{L_A}}{\partial n}\right|_q \left.\frac{\partial n}{\partial \alpha}\right|_q \tag{12}$$

Observe the subscripts for constant q and n. Now it is seen from Eq. (10) that

$$\left.\frac{\partial n}{\partial \alpha}\right|_q = \frac{\partial n}{\partial C_{L_A}}\bigg|_q \left.\frac{\partial C_{L_A}}{\partial \alpha}\right|_q = \frac{C_{L_{\alpha_A}}}{C_{L_{\text{trim}}}} \tag{13}$$

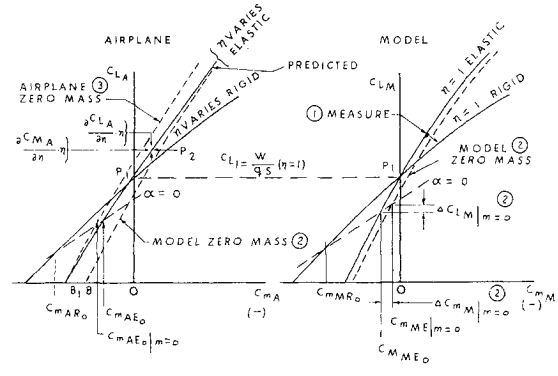

Fig. 12 Prediction of airplane pitching-moment curve from elastic model data.

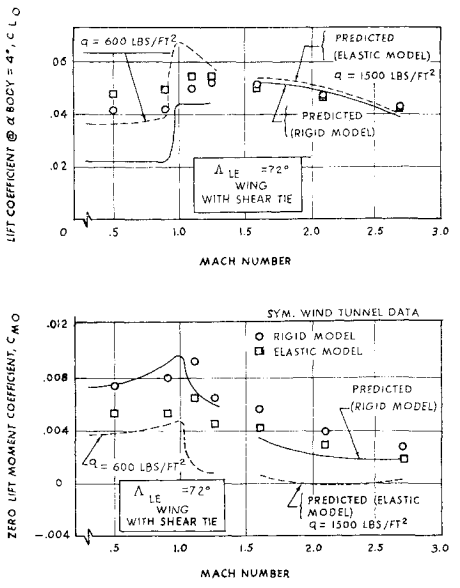

Fig. 13 Correlation of theoretical and experimental C_{L_0} and C_{m_0}.

so by substituting into Eq. (12)

$$C_{L\alpha_A} = \frac{C_{L_{\text{trim}}}}{C_{L_{\text{trim}}} - \partial C_{L_A}/\partial n|_q} C_{L\alpha}|_n \qquad (14)$$

This equation indicates that if the effect of mass distribution on C_L is negligible, then $C_{L\alpha_A} = C_{L\alpha}|_n$, which is to be expected. The equation also demonstrates the fact that $C_{L\alpha_A}$ can be increased or decreased due to the inertial effects, depending on the sign of $\partial C_L/\partial n|_q$. The sign of $\partial C_L/\partial n|_q$ depends on the relative locations of center-of-mass loci to elastic axis. When $\partial C_L/\partial n|_q$ is positive (center of mass behind elastic axis) and larger than $C_{L_{\text{trim}}}$, the airplane lift-curve slope has reversed. Observe that this reversal is different (but, of course, just as undesirable) from the reversal of the constant load factor (zero mass) lift-curve slope $C_{L\alpha_n}$.

5) Observe that Eq. (14) can account for nonlinear effects, provided $C_{L\alpha_n}$ is measured at the proper trim angle of attack on the elastic model.

6) In view of the smallness of $\Delta C_{L_{M\ m=0}}$, step 2 can be eliminated.

For arbitrary (other than cruise or design) flight conditions, the rigid model still has a shape corresponding to the cruise shape. Therefore, this shape no longer corresponds to that of the airplane if it is frozen at the new flight condition. It seems reasonable to assume that this change in shape does not affect $C_{L\alpha}$ to an appreciable extent. In other words, this shape change affects the camber and twist distribution but not $C_{L\alpha}$. Therefore, the rigid model will still give the correct lift-curve slope. The change in camber and twist distribution on the airplane can be estimated by computing the equilibrium shape of the airplane at the new flight condition. By subtracting this estimate from the known camber and twist distribution at the design flight condition, an incremental value is obtained. This incremental camber and twist distribution is responsible for an increment in lift coefficient ΔC_{LCTW}. This quantity can be determined from aerodynamic influence coefficient theory. The corrected rigid model (and therefore rigid airplane) $C_{L_M} - \alpha$ curve can now be obtained by shifting the measured curve vertically over ΔC_{LCTW}. The remaining procedures in predicting the full-scale airplane $C_{L_A} - \alpha$ curve are identical to those outlined for the design flight condition.

The question can be raised as to what should be done to correct for flexibility effects on the so-called rigid model. In general, such corrections are expected to be small. Therefore, theoretically obtained aeroelastic model corrections

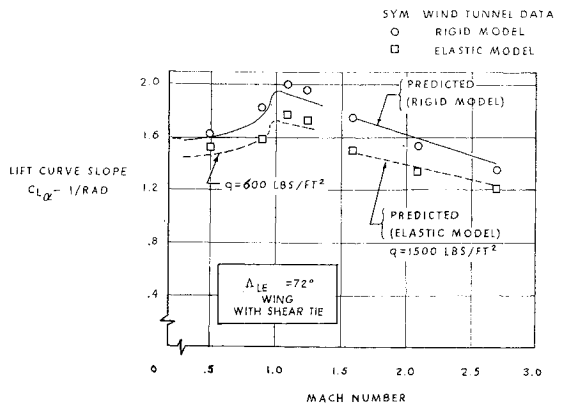

Fig. 14 Correlation of theoretical and experimental lift-curve slope $C_{L\alpha}$.

should be accurate. Such corrections can be computed as soon as a flexibility matrix is obtained for the model. Such a matrix can be computed as follows: 1) directly from the known model structure (this means an enormous amount of work and is probably not worth it); 2) indirectly from measurement of EI and GJ distributions and applications of beam theory (this has also been done with elastic models to verify estimated stiffness properties); and 3) indirectly by measuring influence coefficients at specified control points (this could be a check on 2 to see if that approach is sufficiently accurate).

Ideally then, all model $C_{L_M} - \alpha$ data should be corrected for flexibility effects, after which the data can be used as representative of a truly rigid model in the manner previously described.

6.2 Prediction of Pitching Moment vs Lift-Coefficient Curve from Elastic Model Data

This section describes four steps needed to predict the full-scale $C_L - C_m$ curve for an airplane using elastic model data. The measured rigid and elastic model pitching-moment curves are shown in Fig. 12 (step 1). By computing $\Delta C_{L_{M\ m=0}}$ (as before) and $\Delta C_{m_{M\ m=0}}$ for the elastic model, it is possible to construct the zero-mass model pitching-moment curve. In Sec. 6.1 it was already shown that $\Delta C_{L_{M\ m=0}}$ can be expected to be negligible. The same is true for $\Delta C_{m_{M\ m=0}}$, a typical value for which is -0.00010 at $M = 2.7$ and $q = 456$ psf. This number is indeed small compared with the corresponding airplane value at the same flight condition, which is $\Delta C_{L_{M\ m=0}} = -0.00305$.

In any case, the zero-mass model curve in Fig. 12 can now be obtained by shifting along a constant α line. This assumes that the increments $\Delta C_{L_{M\ m=0}}$ and $\Delta C_{L_{M\ m=0}}$ are constant with α, which, particularly in view of their smallness, is justified. This terminates step 2.

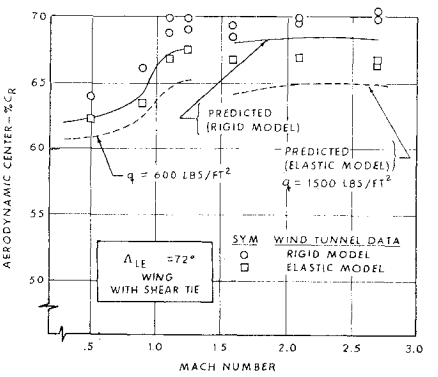

Fig. 15 Correlation of theoretical and experimental aerodynamic center ac.

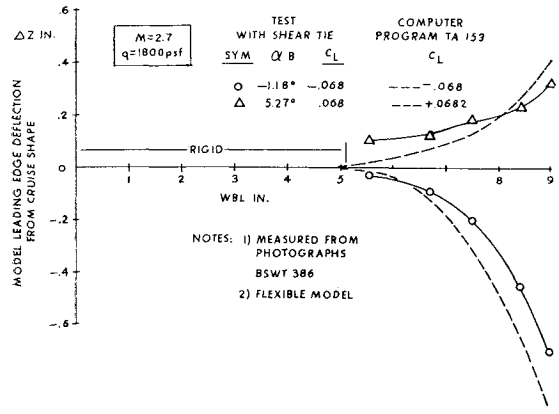

Fig. 16 Correlation of theoretical and experimental deformation.

For the elastic airplane, the zero-mass pitching-moment curve can be found by establishing point P_2 from calculations of $\partial C_{L_A}/\partial n$ and $\partial C_{m_A}/\partial n$. Neither of these values is negligible. By shifting the zero-mass model curve along a constant α line until it intersects P_2, it is possible to find point B_1, step 3. At point B_1, the true airplane has zero load factor, and therefore the elastic zero-mass and full-mass lines intersect here. By adding the increment $\partial C_{m_A}/\partial n$ to the zero-mass curve, it is now possible to draw in the predicted airplane pitching-moment curve, which will go through points B_1 and P_1. This completes step 4 and terminates the procedure required for prediction of elastic airplane $C_{L_A} - C_{m_A}$ characteristics.

7. Data Correlation

In this section, correlation between results obtained with flexible models and with theoretical calculations will be discussed. The theoretical methods used employed a straightforward application of aerodynamic and structural influence coefficient methods. Examples of how these methods were applied are discussed in detail in Refs. 1 and 2.

Typical correlations of experimental data and program results are shown in Figs. 13–16 for C_{L_0}, C_{m_0}, C_{L_α}, aerodynamic center location, and actual deformations. The C_{L_0} and C_{L_α} correlations are good; correlation of C_{m_0} is poor. Aerodynamic center correlations, as demonstrated in Fig. 15, are reasonable. The correlation of predicted with measured deformation is good. In all cases the incremental effect due to aeroelasticity as predicted theoretically agrees well with the measurements on the elastic model.

8. Conclusions

It has been demonstrated that elastic models for full-scale dynamic-pressure testing are feasible. Correlation of computed aeroelastic effects on stability characteristics and deformation magnitudes with measured data on the elastic models has been shown to be quite good, in particular where aeroelastic increments are concerned.

References

[1] Roskam, J., "Equations of Motion for Elastic Airplanes I," *Proceedings of the Seminar on Elastic Airplane Stability, Control and Response,* The University of Kansas, Lawrence, Kansas, June 10–14, 1968.

[2] Roskam, J., "Stability Derivatives for Elastic Airplanes: Interpretation and Use," *Proceedings of the Seminar on Elastic Airplane Stability, Control and Response,* The University of Kansas, Lawrence, Kansas, June 10–14, 1968.